Journal of Magnetic Resonance **148,** 238–247 (2001)
doi:10.1006/jmre.2000.2243, available online at http://www.idealibrary.com on IDEAL®

Double-Quantum Excitation in the NMR of Spinning Solids by Pulse-Assisted Rotational Resonance

T. Karlsson,[1] C. E. Hughes, J. Schmedt auf der Günne, and M. H. Levitt[2]

Division of Physical Chemistry, Arrhenius Laboratory, Stockholm University, S-106 91 Stockholm, Sweden

Received January 13, 2000; revised October 26, 2000

We describe a new technique for double-quantum excitation in magic-angle-spinning NMR of powdered solids. The technique is designed to efficiently excite double-quantum coherence in the vicinity of a rotational resonance condition. The offset from rotational resonance allows the double-quantum filtered signals to be observed with high resolution and sensitivity. The method uses rotational excitation of zero-quantum coherence, assisted by radiofrequency pulse cycles. The zero-quantum coherence is converted into double-quantum coherence by a frequency-selective inversion sequence. Experiments on [$^{13}C_2$, ^{15}N]-glycine demonstrate a double-quantum filtering efficiency of $\simeq$41% at a sample rotation frequency of 8.300 kHz, which is 1.600 kHz away from the $n = 1$ rotational resonance. We achieve 32% double-quantum filtering efficiency at a spinning frequency of 9.250 kHz, which is 2.550 kHz away from rotational resonance.

Key Words: **multiple-quantum coherence; double-quantum coherence; zero-quantum coherence; rotational resonance; spin echoes; magic-angle spinning.**

INTRODUCTION

Several methods have been proposed for excitation of double-quantum coherence in powdered solids under magic-angle spinning (*1–10*). These methods have been employed in the context of internuclear distance estimations (*1–8, 11*) and in the determination of molecular torsional angles (*12–18*). Most of these schemes employ intense radiofrequency (RF) irradiation at the Larmor frequency of the recoupled spin species. In most cases, a strong decoupling field must also be applied simultaneously at the Larmor frequency of a second spin species (commonly protons). The RF field amplitudes are often proportional to the sample rotation frequency, making double-quantum excitation difficult at high spinning frequencies due to limited probe performance. In systems with large internuclear distances, long double-quantum excitation and reconversion intervals are necessary and the efficiency is degraded by pulse imperfections.

Recently we presented a technique (*19*) for excitation of double-quantum coherence exploiting rotational resonance (*20–28*). This method uses zero-quantum coherences which are mechanically excited by the sample rotation. The mechanically excited zero-quantum coherences are converted into double-quantum coherences by frequency-selective spin inversion. The method has been shown to be very effective, even in molecular systems with a fairly large internuclear distance (*19*). The technique has also been applied to systems of more than two spins (*29*). However, the overall signal amplitude in this experiment is degraded by the necessity of acquiring the NMR signals under rotational resonance conditions. The spectral peaks are broadened or split by the homonuclear dipole–dipole couplings (*20–27*).

In this article, we show that it is possible to achieve mechanical excitation of zero-quantum coherence, and hence double-quantum coherence, at a spinning frequency which is displaced from rotational resonance. This is done by manipulating the zero-quantum dynamics of the coupled spins by inserting RF cycles, as in the rotational resonance echo schemes (*30, 31*). Most of the spin evolution is still performed without applied RF fields, reducing problems associated with proton decoupling. At the same time, the signal detection is performed off rotational resonance, which improves the resolution and sensitivity.

We present results on [$^{13}C_2$, ^{15}N]-glycine, spinning at 8.300 kHz in a field of 4.7 T, which is 1.700 kHz away from the $n = 1$ rotational resonance (6.700 kHz). The experimental double-quantum excitation efficiency at this spinning frequency was $\simeq$41%. At a sample rotation frequency of $\omega_r/2\pi = 9.250$ kHz, which is 2.650 kHz away from the $n = 1$ rotational resonance, we achieve $\simeq$32% double-quantum excitation efficiency for the same sample.

PULSE SEQUENCES

The pulse sequences in Fig. 1 are suitable for double-quantum excitation in the magic-angle spinning (MAS) of powdered solids containing isolated pairs of spin-1/2 nuclei. The top row *I* denotes RF fields applied at the Larmor frequency of the abundant spin species, commonly protons. The rows a and b represent two alternative schemes applied at the

[1] Present address: Department of Chemistry, University of Washington, Seattle, WA 98195.

[2] To whom correspondence should be addressed. E-mail: mhl@physc.su.se.

1090-7807/01 $35.00

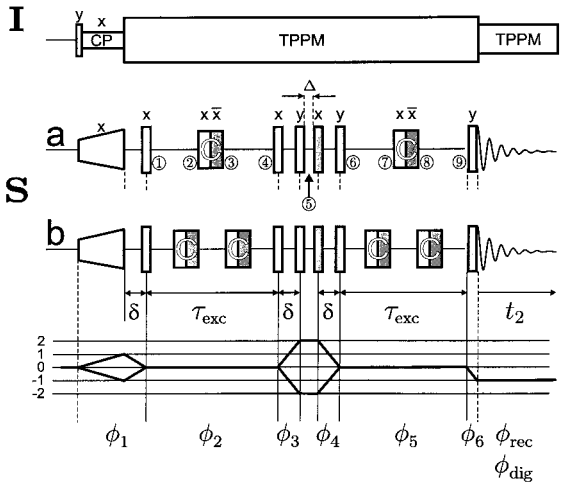

FIG. 1. Pulse sequences for the off rotational resonance excitation of double-quantum coherence and associated coherence transfer pathway diagram.

Larmor frequency of the dilute *S*-spins, typically ^{13}C or ^{31}P nuclei. Scheme a is used relatively close to rotational resonance, while scheme b may be used further away from rotational resonance (see below). The appropriate choice of spinning frequency for these two schemes is discussed under Theory. The bottom row is a coherence transfer pathway diagram for the *S*-spins.

The symbols $\phi_1 \ldots \phi_6$, ϕ_{rec} denote the overall RF phases of pulse sequence blocks. The symbol ϕ_{dig} denotes the postdigitization phase shift (*32*). All of these symbols take into account the sign of the Larmor frequency and the mixing scheme of the RF signals, as discussed in Refs. (*32, 33*).

The pulse sequences start by ramped cross-polarization (*34*) with phase $\phi = 0$ to achieve enhanced transverse *S*-spin magnetization along the *x* axis of the rotating reference frame. Free precession of transverse magnetization occurs under the subsequent delay δ. If the spectrometer reference frequency is set to the mean of the two isotropic shift frequencies, $\omega_{ref} = \frac{1}{2}(\omega_j^{iso} + \omega_k^{iso})$ and the delay is given by $\delta = |\pi/(\omega_j^{iso} - \omega_k^{iso})|$, the $\pi/2$-pulse generates longitudinal difference magnetization, i.e., positive *z* magnetization for one of the two coupled sites and negative *z* magnetization for the other. This sequence neglects chemical shift anisotropy. If the chemical shift anisotropy is considerable, other sequences could be employed instead (*35, 36*).

Mechanical excitation of zero-quantum coherence is accomplished in the following interval τ_{exc}. In Fig. 1a, the interval τ_{exc} is interrupted by a short RF sequence, denoted C. The C sequence is composed of two pulses of equal duration, but with opposite RF phases. The total duration of the sequence C depends on the sample rotation frequency ω_r and the closest rotational resonance condition. If the spinning frequency is close to the first-order rotational resonance ($|\omega_j^{iso} - \omega_k^{iso}| \simeq \omega_r$), then the duration of C is set to one-half of a rotational period, $\tau_C = \tau_r/2$, where $\tau_r = |2\pi/\omega_r|$.

Ideally, the C sequence acts as a *cycle*, meaning that it leaves the spins unperturbed if all interactions other than the RF field are neglected (*37*). Since the cycle has a finite duration, the orientation of the rotating sample is different before and after the cycle, which causes modified spin dynamics in the subsequent interval. This idea has been used before to excite rotational resonance echoes (*30, 31*) and for sideband suppression (*38*).

The purpose of the C sequence in this experiment is to assist the excitation of zero-quantum coherence. In Fig. 1a, the interval τ_{exc} is divided into two intervals, τ, separated by a single C element of duration τ_C (Fig. 2). The optimum value of τ_{exc} is determined by the effective dipole–dipole coupling between the two spins, S_j and S_k, and the sample rotation frequency, ω_r, as discussed below.

After the zero-quantum excitation delay τ_{exc}, two $\pi/2$-pulses, with phases $\phi = 0$ and $\phi = \pi/2$, follow with an intermediate delay δ. This two-pulse sequence selectively rotates the spins in one of the sites by π, converting the zero-quantum coherence into double-quantum coherence.

After a short delay Δ, double-quantum coherence is converted back into zero-quantum coherence by a similar two-pulse sequence. The delay Δ is adjusted such that the interval between timepoint ④ and timepoint ⑥ is an integer number of rotor periods.

The following interval τ_{exc}, including the C sequence, converts the zero-quantum coherence back into a state of longitudinal difference magnetization. The last $\pi/2$-pulse generates transverse magnetization, which is observed in the interval t_2.

A strong ^1H decoupler field is employed throughout the double-quantum excitation and reconversion sequence. In the experiments described here, we employed a TPPM modulation scheme (*39*) in order to improve the quality of the decoupling.

The sequence in Fig. 1b is designed to operate at a sample rotation frequency farther away from the rotational resonance condition. Both intervals τ_{exc} are divided into three subintervals, each of duration τ, separated by two C elements. The

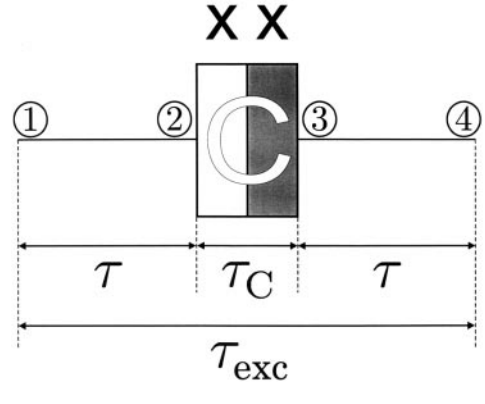

FIG. 2. Expansion of the interval τ_{exc} in Fig. 1a.

duration of the C elements is chosen in the same way as for the sequence in Fig. 1a.

The signal passing through double-quantum coherence at time point ⑤ is collected by cycling the phases of the pulse sequence blocks according to standard procedures (*40*). The phases of the pulse sequence blocks $\phi_1, \phi_2, \ldots, \phi_6$ and the RF receiver phase ϕ_{rec} are cycled according to

$$\phi_1 = \phi_1^0 + \frac{2\pi m}{n_1}$$

$$\phi_p = \phi_p^0 + \frac{2\pi}{n_p}\,\text{floor}\left(\frac{m}{n_1 n_2 \ldots n_{p-1}}\right), \quad (\text{for } 2 \le p \le 6)$$

$$\phi_{\text{rec}} = \frac{2\pi m}{4}, \qquad [1]$$

where the function floor (x) returns the largest integer not greater than x. Here m is the transient counter, $m = 0, 1, \ldots, n_{\text{tot}} - 1$, where n_{tot} is the number of transients in a complete phasecycle, $n_{\text{tot}} = n_1 n_2 n_3 n_4 n_5 n_6$. In the present case, the cycling parameters were $n_1 = 1$; $n_2 = 1$; $n_3 = 1$; $n_4 = 4$; $n_5 = 1$; $n_6 = 2$; $n_{\text{rec}} = 4$; $n_{\text{tot}} = 8$. On each transient, the postdigitization phase ϕ_{dig} was adjusted to satisfy the equation

$$\phi_{\text{dig}} = -2\phi_3 + 2\phi_4 + \phi_6 - \phi_{\text{rec}}. \qquad [2]$$

This phase cycle selects signals passing through (± 2)-quantum coherence at time point ⑤ in Fig. 1. The initial phases $\phi_1^0, \phi_2^0, \ldots, \phi_6^0$ were all set to zero, except for ϕ_4^0, which was optimized experimentally to obtain maximum 2Q filtering efficiency (see below).

THEORY

Zero-Quantum Dynamics

The theoretical treatment of these experiments is similar to that for the on rotational resonance case, explored in Ref. (*19*). Both experiments may be treated using a fictitious spin-1/2 formalism in the zero-quantum subspace.

The high field MAS Hamiltonian for an isolated spin pair in a rotating solid may be written as (*23*)

$$H = H^0 + H^{23}, \qquad [3]$$

where

$$H^0 = \omega_\Sigma^{\text{iso}} S_z^{14} + \omega_A (S_z^{12} - S_z^{34}) \qquad [4]$$

$$H^{23} = \omega_\Delta^{\text{iso}} S_z^{23} + \omega_B S_x^{23} \qquad [5]$$

and the CSA interaction is ignored for simplicity.

The terms $\omega_\Sigma^{\text{iso}}$ and $\omega_\Delta^{\text{iso}}$ represent the sum of the instantaneous chemical shift frequencies, i.e., $\omega_\Sigma^{\text{iso}} = \omega_j^{\text{iso}} + \omega_k^{\text{iso}}$, $\omega_\Delta^{\text{iso}} = \omega_j^{\text{iso}} - \omega_k^{\text{iso}}$. The terms ω_A and ω_B are orientation-dependent and represent different components of the spin–spin coupling (see Ref. (*19*)).

Equations [4] and [5] employ single-transition operators (*41*), using the basis set $|1\rangle = |+\tfrac{1}{2}, +\tfrac{1}{2}\rangle$, $|2\rangle = |+\tfrac{1}{2}, -\tfrac{1}{2}\rangle$, $|3\rangle = |-\tfrac{1}{2}, +\tfrac{1}{2}\rangle$, $|4\rangle = |-\tfrac{1}{2}, -\tfrac{1}{2}\rangle$. The relevant spin dynamics during the interval τ_{exc} are governed by the homogeneous part of the Hamiltonian, H^{23} (Eq. [5]), which represents the interaction of the spin system with a pseudo-field in the $\{|2\rangle, |3\rangle\}$-subspace (zero-quantum space) (*23*). The pseudo-field has a longitudinal component, $\omega_\Delta^{\text{iso}}$, and a transverse component, ω_B. The longitudinal component $\omega_\Delta^{\text{iso}}$ is both time- and orientation-independent in the absence of CSA. The transverse component ω_B is orientation-dependent and also time-dependent due to the sample rotation. It is convenient to represent ω_B as a Fourier series,

$$\omega_B(t, \Omega^{\text{MR}}) = \sum_{m=-2}^{+2} \omega_B^{(m)}(\Omega^{\text{MR}}) e^{im\omega_r t}, \qquad [6]$$

where the orientation-dependent Fourier components are given in Ref. (*19*).

The zero-quantum part of the spin density operator may be described by a fictitious spin-1/2 vector, denoted by ρ^{23}, precessing around the pseudo-field. The component ρ_z^{23} corresponds to longitudinal difference magnetization, while the transverse components, ρ_x^{23} and ρ_y^{23}, correspond to zero-quantum coherences.

At rotational resonance ($\omega_\Delta^{\text{iso}} = n\omega_r$), the frequency of the nth Fourier component of ω_B matches the frequency $\omega_\Delta^{\text{iso}}$. The magnitude and phase of the on-resonant Fourier component are denoted B_n and ϕ_n, with

$$\omega_B^{(n)} = B_n e^{i\phi_n}. \qquad [7]$$

The real quantities, B_n and ϕ_n, are orientation-dependent and are given in Ref. (*19*).

At rotational resonance, ρ^{23} describes a complicated spiral trajectory. A simplified picture is obtained by transforming into a frame which rotates at the frequency ω_r in the case of $n = 1$ rotational resonance (*31*). If off-resonant terms are ignored, the zero-quantum vector ρ^{23} nutates around a time-independent transverse field of magnitude B_n and phase ϕ_n (Fig. 3a). In the following equations, the use of the zero-quantum rotating frame is denoted by the symbol $\sim$. The zero-quantum density operators in the laboratory frame and zero-quantum rotating frame are related by $\tilde{\rho}^{\text{ZQ}}(t) = R_z^{23}(-\omega_r t)\rho^{\text{ZQ}}(t) R_z^{23}(+\omega_r t)$.

If the experiment is conducted off rotational resonance, the zero-quantum dynamics may be described by a nutation about a tilted field, denoted ω_{eff} in Fig. 3b. The tilt angle θ and the nutation frequency ω_{eff} depend on the sample rotation frequency and are given by

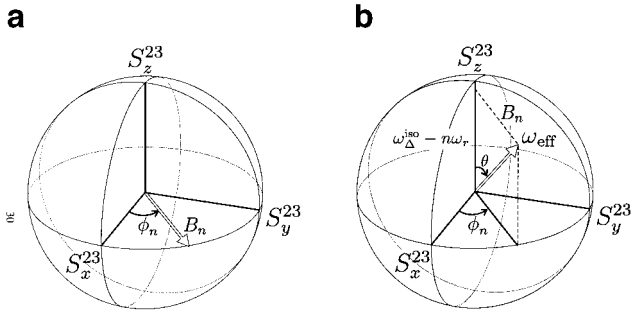

FIG. 3. Effective fields in the rotating zero-quantum frame; (a) at exact rotational resonance and (b) off rotational resonance.

$$\theta = \tan^{-1}\left(\frac{B_n}{|\omega_\Delta^{iso} - n\omega_r|}\right) \quad [8]$$

$$\omega_{eff} = \{(\omega_\Delta^{iso} - n\omega_r)^2 + B_n^2\}^{1/2}. \quad [9]$$

In a powder, a distribution of phases, nutation frequencies, and tilt angles is present.

Pulse-Assisted Excitation of Zero-Quantum Coherence

Figure 2 shows the interval τ_{exc} on an expanded scale. The total interval is given by $\tau_{exc} = 2\tau + \tau_C$, where τ_C is the duration of the cycle C. If $\tau_C = \frac{1}{2}\tau_r$, and the spinning frequency is close to the $n = 1$ rotational resonance, then the cycle C rotates the fictitious spin-1/2 vector (*31*) through the angle $-\pi$ about the z-axis of the zero-quantum rotating frame, as described in Ref. (*19*).

In Figs. 4a–4d, the desired spin dynamics during τ_{exc} is visualized for a single molecular orientation, neglecting the chemical shift anisotropy. The effective field ω_{eff} (white arrow) and the fictitious magnetization vector (black arrow) are shown. The effective field is in the yz plane.

The $\tilde{\rho}^{23}$ vector is initially along the S_z^{23}-axis, denoting longitudinal difference magnetization, (time point ① in Fig. 1a). The relevant part of the density matrix in the zero-quantum rotating frame may be written

$$\tilde{\rho}_{①}^{ZQ} \simeq \frac{1}{2}(S_{jz} - S_{kz}) = S_z^{23}, \quad [10]$$

neglecting inessential factors.

During the first period τ, $\tilde{\rho}^{23}$ rotates about the pseudo-field ω_{eff} through an angle β, given by

$$\beta = \omega_{eff}\tau. \quad [11]$$

If relaxation is ignored, the relevant part of the density matrix at time point ② is given by

$$\tilde{\rho}_{②}^{ZQ} \simeq \sin\beta\sin\theta S_x^{23} + (1 - \cos\beta)\cos\theta\sin\theta\, S_y^{23} + (\cos^2\theta + \cos\beta\sin^2\theta)S_z^{23}. \quad [12]$$

In Fig. 4a, this evolution is shown for the case that $\beta = \pi$.

The cycle C acts as a rotation of the $\tilde{\rho}^{23}$ vector by $-\pi$ about the z-axis of the zero-quantum rotating frame, S_z^{23} (Fig. 4b). The relevant part of the density matrix after the cycle C is therefore

$$\tilde{\rho}_{③}^{ZQ} \simeq -\sin\beta\sin\theta S_x^{23} - (1 - \cos\beta)\cos\theta\sin\theta\, S_y^{23} + (\cos^2\theta + \cos\beta\sin^2\theta)S_z^{23}. \quad [13]$$

After release from the cycle C (time point ③ to time point ④), the fictitious spin-1/2 again nutates through an angle $\beta = \omega_{eff}\tau$ about the tilted field (Fig. 4c).

The zero-quantum components of the density operator at timepoint ④ are

$$\tilde{\rho}_{④}^{ZQ} = 2\cos\theta\sin(2\theta)\sin\beta\sin^2\left(\frac{\beta}{2}\right)S_x^{23} + \frac{1}{2}\left(4\cos(2\theta)\sin^4\left(\frac{\beta}{2}\right) - \sin^2\beta\right)\sin 2\theta\, S_y^{23} + \left(1 - 2\sin^2(2\theta)\sin^4\left(\frac{\beta}{2}\right)\right)S_z^{23}. \quad [14]$$

If the tilt of the effective field is adjusted such that $\theta = \pi/8$ and the nutation angles are adjusted to be $\beta = \pi$, then the $\tilde{\rho}^{23}$ vector ends up along the y-axis as shown in Fig. 4d. This corresponds to a perfect conversion of longitudinal difference magnetization into zero-quantum coherence. Note that the $\tilde{\rho}^{23}$ vector would return to the z-axis during the second interval τ, if the cycle C were not applied.

In a powder, the distribution in the magnitude of the effec-

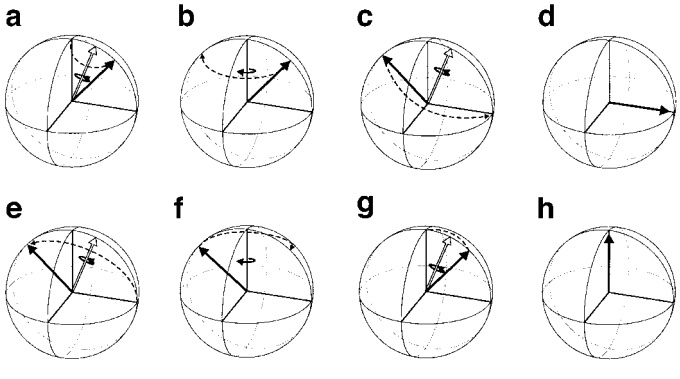

FIG. 4. Spin dynamics in the rotating zero-quantum frame under the pulse sequence in Fig. 1a. Frames (a) to (d) denote excitation of zero-quantum coherence. Frames (e) to (h) denote reconversion of zero-quantum coherence into longitudinal difference magnetization. Black arrows denote the magnetization; white arrows denote the field.

tive field ω_{eff} and the tilt angles θ makes it impossible to achieve optimum zero-quantum excitation for all molecular orientations at the same time. Nevertheless, the rotation sequence in Figs. 4a–4d may be set up for the most probable value of the near-resonant dipolar component (*2*). In the case $n = 1$, this is given by $B_n^{\text{most prob}} \simeq b_{jk}/(2\sqrt{2})$, where $b_{jk} = -(\mu_0/4\pi)\gamma_j\gamma_k\hbar/r_{jk}^3$ is the dipole–dipole coupling constant expressed in rad s^{-1} and r_{jk} is the internuclear distance. This value of B_n occurs for molecular orientation angles $\beta_{\text{MR}} = \pi/4$ and $3\pi/4$. Close to the $n = 1$ rotational resonance, this corresponds to a choice of spinning frequency

$$\omega_{\text{r}} \simeq |\omega_j^{\text{iso}} - \omega_k^{\text{iso}}| \pm \left| \frac{b_{jk}}{2\sqrt{2}\,\tan(\pi/8)} \right| \qquad [15]$$

and intervals

$$\tau \simeq \left| \frac{2\sqrt{2}\,\pi}{b_{jk}} \right| \sin(\pi/8) \qquad [16]$$

$$\tau_{\text{C}} = \frac{1}{2}\,\tau_{\text{r}}. \qquad [17]$$

The spread of different field magnitudes and tilt angles degrades the double-quantum filtering efficiency in a powder. However, the distribution in the *phase* of the pseudo-field, associated with the Euler angle γ_{MR}, is not harmful for the zero-quantum excitation. The trajectories for molecular orientations with different values of the Euler angle γ_{MR} may be generated by rotating the pictures in Fig. 4 about the z-axis.

In another context, strong nonselective π-pulses were used to improve the exchange dynamics of longitudinal difference magnetization in pairs of spins-1/2 off rotational resonance (*42, 43*). However, this method depends on the phase of the effective field and hence on the angle γ_{MR}. As a result, the methods in Refs. (*42, 43*) are relatively inefficient in a powder.

Excitation of Double-Quantum Coherence

The following four $\pi/2$-pulses, time point ④ ⇒ ⑥ in Fig. 1a, convert zero-quantum coherence into double-quantum coherence and vice versa.

If chemical shift anisotropy and dipole–dipole couplings are neglected over the short interval δ, the arguments given in Ref. (*19*) may be repeated to write the effect of the two-pulse sequence in the conventional rotating frame:

$$U_{2\text{P}} \simeq R_{jz}\left(\frac{\pi}{2}\right) R_{jx}(\pi)\, R_{kz}\left(-\frac{\pi}{2}\right), \qquad [18]$$

assuming that the spectrometer reference frequency is set to the mean of the two isotropic shift frequencies and that the delay δ is chosen to be $\delta = \pi/\omega_\Delta^{\text{iso}}$. The single-spin rotation operators are given by

$$R_{j\mu}(\beta) = \exp\{-i\beta S_{j\mu}\}. \qquad [19]$$

Suppose that the zero-quantum part of the spin density operator, in the zero-quantum rotating frame, is given at time point ④ by

$$\tilde{\rho}^{\text{ZQ}}{}_{④} \simeq A\,\frac{1}{2}\,(e^{i\phi^{\text{ZQ}}} S_j^- S_k^+ + e^{-i\phi^{\text{ZQ}}} S_j^+ S_k^-), \qquad [20]$$

where A and ϕ^{ZQ} are the amplitude and the phase of the excited zero-quantum coherence. The corresponding expression for the zero-quantum density operator in the usual rotating frame is

$$\rho^{\text{ZQ}}{}_{④} \simeq A\,\frac{1}{2}\,(S_j^- S_k^+ \exp\{i(\phi^{\text{ZQ}} + \omega_{\text{r}} t_④)\} + S_j^+ S_k^- \exp\{-i(\phi^{\text{ZQ}} + \omega_{\text{r}} t_④)\}). \qquad [21]$$

The two-pulse sequence leads to the following double-quantum spin density operator:

$$\rho_⑤^{\text{DQ}} = U_{2\text{P}} \rho_④^{\text{ZQ}} U_{2\text{P}}^{-1} \qquad [22]$$

$$\simeq A\,\frac{1}{2}\,(e^{i\phi^{\text{DQ}}} S_j^+ S_k^+ + e^{-i\phi^{\text{DQ}}} S_j^- S_k^-), \qquad [23]$$

where

$$\phi^{\text{DQ}} = \phi^{\text{ZQ}} + \omega_{\text{r}} t_④. \qquad [24]$$

This represents the conversion of zero-quantum into double-quantum coherence, with faithful transfer of the phase information.

If the spectrometer reference frequency is set to the mean of the two isotropic shift frequencies, and chemical shift anisotropy is neglected, then there is no precession of double-quantum coherence during the interval Δ.

Reconversion of Double-Quantum Coherence

The second two-pulse sequence is the same as the first and transforms the excited double-quantum coherences back into zero-quantum coherence. The zero-quantum part of the spin density operator at time point ⑥ is therefore

$$\rho_⑥^{\text{ZQ}} = A\,\frac{1}{2}\,(S_j^- S_k^+ \exp\{i(\phi^{\text{ZQ}} + \omega_{\text{r}} t_④)\} + S_j^+ S_k^- \exp\{-i(\phi^{\text{ZQ}} + \omega_{\text{r}} t_④)\}). \qquad [25]$$

Transforming back into the zero-quantum rotating frame, we get

$$\tilde{\rho}_{⑥}^{ZQ} = A\,\frac{1}{2}\,(S_j^- S_k^+ \exp\{i(\phi^{ZQ} + \omega_r t_④ - \omega_r t_⑥)\} + S_j^+ S_k^- \exp\{-i(\phi^{ZQ} + \omega_r t_④ - \omega_r t_⑥)\}). \quad [26]$$

The delay Δ is chosen such that the time points ④ and ⑥ are separated by an integer number of rotational periods. Under these conditions, the term $\omega_r(t_④ - t_⑥)$ may be neglected and the zero-quantum coherence is reconstructed at time point ⑥ with complete preservation of phases.

A Zero-Quantum Echo

During the interval ⑥ ⇒ ⑨, the zero-quantum coherence is reconverted into longitudinal difference magnetization. This process is visualized for a single molecular orientation in Fig. 4e ⇒ Fig. 4h. In a powder, the simultaneous refocussing of many zero-quantum vectors at the z-axis represents an echo of longitudinal difference magnetization (*30, 31*).

Further Away from Rotational Resonance

Improved spectral resolution is obtained if the sample rotation frequency is set further away from the rotational resonance condition. In theory, this makes double-quantum excitation more difficult, since the tilt angle θ of the effective field ω_{eff} in the zero-quantum frame becomes smaller (Fig. 2). To compensate for this, one may insert more RF cycles C in the intervals τ_{exc}. A pulse sequence with two cycles is shown in Fig. 1b. Each interval τ_{exc} is divided into three subintervals, τ, separated by two cycles, C, so that $\tau_{exc} = 3\tau + 2\tau_C$. Approximate optimal settings for this sequence, based on the trajectory of the $\tilde{\rho}^{23}$ vector for the most probable component of the resonant dipole–dipole coupling, are given by

$$\omega_r \simeq |\omega_j^{iso} - \omega_k^{iso}| \pm \left|\frac{b_{jk}}{2\sqrt{2}\,\tan(\pi/12)}\right| \quad [27]$$

$$\tau \simeq \left|\frac{2\sqrt{2}\,\pi}{b_{jk}}\right| \sin(\pi/12) \quad [28]$$

$$\tau_C = \frac{1}{2}\,\tau_r. \quad [29]$$

The geometric arguments in Fig. 4 may readily be extended to show that this sequence also leads to optimal double-quantum excitation for molecular orientations with the most probable value of the recoupled dipolar interaction. The overall efficiency of the sequence with two C cycles in each τ_{exc} interval is lower than that with a single C cycle, because the more complicated evolution leads to increased destructive interference in a powder. However, the increased offset from rotational resonance leads to enhanced resolution.

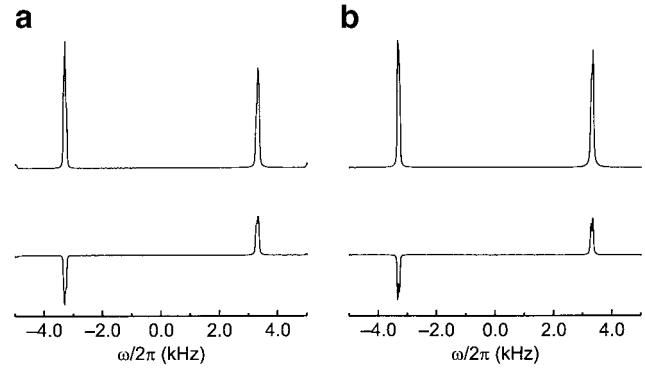

FIG. 5. Excitation of $^{13}C_2$ double-quantum coherence above the $n = 1$ rotational resonance condition in [$^{13}C_2$, ^{15}N]-glycine. The upper spectrum in (a) is an ordinary CP/MAS spectrum, while the lower spectrum is a double-quantum filtered spectrum acquired with the pulse sequence in Fig. 1a. Both spectra were acquired at a sample rotation frequency $\omega_r/2\pi = 8.300$ kHz. The upper spectrum in (b) is a CP/MAS spectrum, while the lower spectrum was acquired with the pulse sequence in Fig. 1b. Both spectra in (b) were acquired at a sample rotation frequency $\omega_r/2\pi = 9.250$ kHz.

Nonidealities

The arguments stated above neglect chemical shift anisotropy, the distribution of molecular orientations, and the durations of the pulses (except for that of the C element). In practice, the intervals τ and the phase ϕ_4^0 are adjusted empirically in order to achieve optimal efficiency.

RESULTS

The spectra in Fig. 5 demonstrate double-quantum excitation in a sample of [$^{13}C_2$, ^{15}N]-glycine. The spectra in Fig. 5a were obtained at a sample rotation frequency $\omega_r/2\pi = 8.300$ kHz in a field of 4.7 T, which is 1.700 kHz above the $n = 1$ rotational resonance condition, which occurs at a spinning frequency of 6.700 kHz. The upper spectrum is an ordinary CP/MAS spectrum, while the lower spectrum is a double-quantum filtered spectrum, acquired with the pulse sequence in Fig. 1a. The pulse sequence parameters were $\tau = 308$ μs, $\Delta = 90.6$ μs, $\tau_C = 60.2$ μs, and $\phi_4^0 = 8°$.

A measure of the double-quantum filtering efficiency is obtained by comparing the peak integrals in the CP/MAS spectrum with the peak integrals in the double-quantum filtered spectrum. The measured peak integrals reveal a double-quantum excitation efficiency of $\simeq$41%.

To illustrate the dependence of the double-quantum excitation efficiency on the sample rotation frequency and the excitation time τ_{exc}, a series of experiments was carried out using the pulse sequence in Fig. 1a (which contains one cycle C) and a similar sequence containing no C cycles. Figure 6 compares

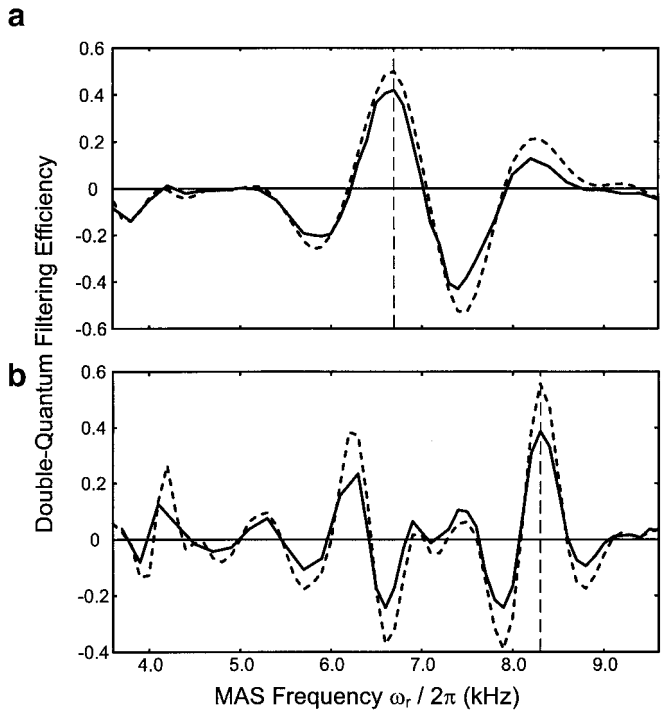

FIG. 6. The dependence of double-quantum filtering excitation in [$^{13}C_2$, ^{15}N]-glycine on the sample rotation frequency. (a) Excitation at the $n = 1$ rotational resonance condition using a pulse sequence similar to that in Fig. 1a but containing no C cycles. Only the spinning frequency was varied. The rotational resonance condition is indicated by the dashed vertical line. (b) Excitation above the $n = 1$ rotational resonance condition using the pulse sequence in Fig. 1a varying only the spinning frequency. The pulse sequence parameters were optimized for the spinning frequency $\omega_r/2\pi = 8.300$ kHz, indicated by the dashed vertical line.

the rotation-frequency dependence of the double-quantum excitation efficiency for the two pulse sequences.

Figure 6a shows the spinning frequency dependence of the double-quantum filtering efficiency for a sequence with no inserted C cycles, optimized at the $n = 1$ rotational resonance. The pulse sequence parameters were $\tau = 350$ μs, $\Delta = 0.5$ μs, and $\phi_4^0 = 0$. The solid curve shows the experimental results, while the dashed curve shows the results of numerical simulations using the SIMPSON program (*44*). The simulations employed a powder average of 8816 crystal orientations and an integral step size of $\tau_r/200$. Other parameters were the same as in the experimental setup. Pulse imperfections and relaxation were ignored in the simulations. The spin Hamiltonian parameters used for the simulations in Figs. 6 and 7 are as follows: $b_{jk}/2\pi = -2.135$ kHz, $\delta_j^{iso} - \delta_k^{iso} = -133.2$ ppm, $\delta_j^{aniso} = -19.4$ ppm, $\eta_j = 0.98$, $\{\alpha_j^{PM}, \beta_j^{PM}, \gamma_j^{PM}\} = \{99.4°, 146.0°, 138.9°\}$, $\delta_k^{aniso} = -74.5$ ppm, $\eta_k = 0.88$, $\{\alpha_k^{PM}, \beta_k^{PM}, \gamma_k^{PM}\} = \{-0.7°, 88.5°, 42.5°\}$, and $J_{jk} = 53.1$ Hz, where a deshielding convention is used throughout for the chemical shifts, the label j refers to the 2-^{13}C site, and the label k refers to the 1-^{13}C site. The z-axis of the molecular reference frame M is along the C–C bond. These parameters were taken from "molecule 1" in Ref. (*45*), except for the isotropic shift difference which was increased in magnitude by 2.2 ppm.

We attribute this small discrepancy to the general difficulty of measuring isotropic chemical shifts in systems with strong dipole–dipole couplings, as well as a possible isotope effect on ^{13}C chemical shifts when substituting an ^{14}N nucleus by ^{15}N. The crystal structures of the two samples may also differ. Simulations using the parameters reported in Ref. (*45*) are in clear discrepancy with our experimental results, while a small adjustment of the isotropic shift difference leads to agreement.

Figure 6a shows a gratifying match between simulations and experimental results. The highest double-quantum filtering efficiency is obtained, as expected, at the rotational resonance condition $\omega_r/2\pi = 6.700$ kHz. Rather surprisingly, intense double-quantum filtered signals, but with opposite sign, are also obtained at $\omega_r/2\pi = 7.400$ kHz, which is 0.700 kHz above rotational resonance.

Figure 6b shows that the insertion of one C cycle in the interval τ_{exc}, as in the pulse sequence in Fig. 1a, leads to displacement of the optimal excitation to a position well off rotational resonance. The pulse sequence parameters were $\tau = 308$ μs, $\Delta = 90.6$ μs, $\tau_C = 60.2$ μs, and $\phi_4^0 = 8°$. The RF field during the sequences C corresponded to a nutation frequency of $|\omega_{nut}^S/2\pi| = 32.4$ kHz. As may be seen, a good match between experiments and simulations is maintained for this pulse sequence. Optimal double-quantum excitation is ob-

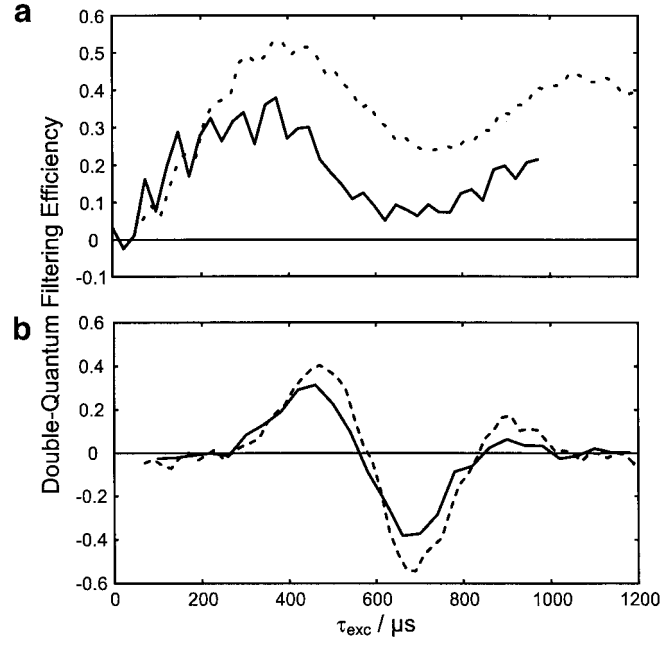

FIG. 7. The dependence of double-quantum filtering efficiency in [$^{13}C_2$, ^{15}N]-glycine on the excitation interval, τ_{exc}. (a) Excitation at the $n = 1$ rotational resonance condition using the pulse sequence in Fig. 1a but containing no C cycles. Only τ_{exc} was varied. Solid lines represent experimental data; dashed lines represent simulations. (b) Excitation above the $n = 1$ rotational resonance condition using the pulse sequence in Fig. 1a and varying the delays τ. The excitation interval τ_{exc} equals $2\tau + \tau_C$.

tained at $\omega_r/2\pi = 8.300$ kHz, as expected. However, the irregular behavior of this pulse sequence with respect to spinning frequency indicates that it should not be relied on to provide a clean frequency-selective excitation of double-quantum coherence.

Further simulations (not shown) predict only a minor dependence of the double-quantum excitation on the RF field amplitude during the sequence C. The simulated double-quantum filtering efficiency has only a weak dependence on the RF field for nutation frequencies that differ from the optimum setting by ± 6 kHz.

Figure 7 shows the dependence of the double-quantum efficiency of the same pair of experiments on the excitation interval τ_{exc}. Figure 7a shows the results for the pulse sequence without C cycles at a sample rotation frequency of 6.600 kHz, which is very close to rotational resonance. Again, there is good agreement with the simulated curves, with the remaining differences being attributable to relaxation. The rapid oscillations in the excitation profile have been observed before (*29*).

Figure 7b shows the corresponding results for the sequence in Fig. 1a, at a sample rotation frequency of 8.300 kHz. A rather sharp maximum in the double-quantum filter efficiency is achieved at $\tau_{exc} = 460$ μs (corresponding to $\tau = 200$ μs). Interestingly, strong excitation (with opposite sign) is also obtained at $\tau_{exc} = 660$ μs (corresponding to $\tau = 300$ μs).

The spectra in Fig. 5b demonstrate double-quantum excitation further away from the rotational resonance condition, using two inserted cycles in both the excitation and the reconversion periods as in Fig. 1b. The upper spectrum in Fig. 5b is an ordinary CP/MAS spectrum acquired at a sample rotation frequency $\omega_r/2\pi = 9.250$ kHz, which is 2.550 kHz above the $n = 1$ rotational resonance condition. The lower spectrum was acquired with the pulse sequence in Fig. 1b. The experimental parameters were $\tau = 199$ μs, $\Delta = 67.0$ μs, $\tau_C = 54.1$ μs, and $\phi_4^0 = 4°$. The peak integrals in this experiment indicate a double-quantum excitation efficiency of $\simeq$32%. The rapid spinning allows the ^{13}C–^{13}C *J*-coupling to be partially resolved in the double-quantum filtered spectrum.

EXPERIMENTAL

[$^{13}C_2$, ^{15}N]-Glycine (98% ^{13}C, 96–99% ^{15}N) was purchased from Cambridge Isotopes and used without further purification or dilution. Approximately 59 mg was packed in a Chemagnetics zirconium oxide rotor with outer diameter 4 mm. The experiments were performed on a Chemagnetics CMX-200 spectrometer operating at a magnetic field of 4.7 T. A Chemagnetics triple-resonance MAS probe with a 4-mm spinner module was used. The spinning frequency was stabilized to ± 2 Hz. The cross-polarization interval was equal to 2 ms in all experiments. The $^{13}C_2$ RF-field intensity was ramped to increase reproducibility (*34*). Typical nutation frequencies during the two-pulse were $|\omega_{nut}^S/2\pi| = 69.4$ kHz on the ^{13}C spins. All spectra in Fig. 5 were acquired using 32 transients, collected with a delay between transients of 3 s. Typical ^{13}C RF-fields during the C sequences corresponded to a nutation frequency of $|\omega_{nut}^S/2\pi| = 32$ kHz. Typical amplitudes of ^1H decoupler fields corresponded to nutation frequencies of $|\omega_{nut}^I/2\pi| = 90$ kHz to 110 kHz. TPPM decoupler schemes were employed with pulse durations of between 4.3 and 6.7 μs and phase alternations of between 6 and 18°.

CONCLUSIONS

The dipolar recoupling technique presented in this article shares many of the features of the experiment discussed in Ref. (*42*), which uses π pulses to achieve recoupling. Both methods employ RF irradiation to compensate for the offset from the rotational resonance condition. However, the current experiment uses RF cycles instead of π pulses, which leads to a reduced orientation dependence and hence better efficiency in a powder.

The off rotational resonance recoupling method could be employed for the determination of internuclear distances in powdered solids and for the generation of double-quantum coherences which may be used in torsional angle estimations (*12–18*). The method allows one to achieve good ZQ-excitation for particular pairs of labeled spins, without suffering from the signal loss associated with rotational resonance splittings.

Other possibilities exist for off rotational resonance excitation of double-quantum coherences. For example, the position of the rotational resonances may be shifted by applying repetitive RF pulses (*46*) or by weak off-resonance RF fields (*26, 28*). Such shifted rotational resonance might be combined with the scheme discussed in Ref. (*19*) to give efficient double-quantum excitation as well as high sensitivity detection.

Several groups have described broadband double-quantum recoupling sequences which are suitable at high spinning frequency (*8, 10*). These methods place high demands on the probe performance but are the methods of choice when simultaneous recoupling of many spins is required or when the precise chemical shift frequencies are unknown. The method described in this paper is selective for pairs of spins satisfying the shifted rotational resonance condition and is relatively undemanding for the probe electronics or the pulse programming device.

We recently used the technique described here to perform NCCN torsional angle estimates in a labeled sample of the tripeptide Gly-Gly-Gly (*47*).

ACKNOWLEDGMENTS

The Swedish National Science Foundation and the Göran Gustafsson Foundation for Research in the Natural Sciences and Medicine are acknowledged for supporting this research. C.E.H. is the recipient of a Marie Curie Individual Fellowship (HPMF-CT-1999-00199) from the European Union. J.S.a.d.G. is supported by the Deutsche Forschungsgemeinschaft (SCHM 1570/1-1). The authors thank Ole G. Johanessen for technical assistance.

REFERENCES

1. R. Tycko and G. Dabbagh, Double-quantum filtering in magic-angle-spinning NMR spectroscopy: An approach to spectral simplification and molecular structure determination, *J. Am. Chem. Soc.* **113,** 9444–9448 (1991).
2. N. C. Nielsen, F. Creuzet, R. G. Griffin, and M. H. Levitt, Enhanced double-quantum nuclear magnetic resonance in spinning solids at rotational resonance, *J. Chem. Phys.* **96,** 5668–5677 (1992).
3. N. C. Nielsen, H. Bildsøe, H. J. Jakobsen, and M. H. Levitt, Double-quantum homonuclear rotary resonance: Efficient dipolar recovery in magic-angle spinning nuclear magnetic resonance, *J. Chem. Phys.* **101,** 1805–1812 (1994).
4. Y. K. Lee, N. D. Kurur, M. Helmle, O. G. Johannessen, N. C. Nielsen, and M. H. Levitt, Efficient dipolar recoupling in the NMR of rotating solids: A seven-fold symmetric radiofrequency pulse sequence, *Chem. Phys. Lett.* **242,** 304–309 (1995).
5. M. Hohwy, H. J. Jakobsen, M. Edén, M. H. Levitt, and N. C. Nielsen, Broadband dipolar recoupling in the nuclear magnetic resonance of rotating solids. A compensated C7 pulse sequence, *J. Chem. Phys.* **108,** 2686–2694 (1998).
6. C. M. Rienstra, M. E. Hatcher, L. J. Mueller, B. Sun, S. W. Fesik, and R. G. Griffin, Efficient multispin homonuclear double-quantum recoupling for magic-angle spinning NMR: ^{13}C–^{13}C correlation spectroscopy of U-^{13}C-erythromycin A, *J. Am. Chem. Soc.* **120,** 10602–10612 (1998).
7. D. M. Gregory, M. A. Mehta, J. C. Shiels, and G. P. Drobny, Determination of local structure in solid nucleic acids using double quantum nuclear magnetic resonance spectroscopy, *J. Chem. Phys.* **107,** 28–42 (1997).
8. M. Hohwy, C. M. Rienstra, C. P. Jaroniec, and R. G. Griffin, Fivefold symmetric homonuclear dipolar recoupling in rotating solids: Application to double quantum spectroscopy, *J. Chem. Phys.* **110,** 7983–7992 (1999).
9. M. Carravetta, M. Edén, X. Zhao, B. A., and M. H. Levitt, Symmetry principles for the design of radiofrequency pulse sequences in the nuclear magnetic resonance of rotating solids, *Chem. Phys. Lett.* **321,** 205–215 (2000).
10. A. Brinkmann, M. Edén, and M. H. Levitt, Synchronous helical pulse sequences in magic-angle spinning NMR. Double quantum recoupling of multiple-spin systems, *J. Chem. Phys.* **112,** 8539–8554 (2000).
11. B.-Q. Sun, P. R. Costa, D. Kocisko, P. T. Lansbury, and R. G. Griffin, Internuclear distance measurements in solid state nuclear magnetic resonance: Dipolar recoupling via rotor synchronized spin locking, *J. Chem. Phys.* **102,** 702–707 (1995).
12. X. Feng, Y. K. Lee, D. Sandström, M. Edén, H. Maisel, A. Sebald, and M. H. Levitt, Direct determination of a molecular torsional angle by solid-state NMR, *Chem. Phys. Lett.* **257,** 314–320 (1996).
13. K. Schmidt-Rohr, Torsion angle determination in solid ^{13}C-labeled amino acids and peptides by separated-local-field double-quantum NMR, *J. Am. Chem. Soc.* **118,** 7601–7603 (1996).
14. X. Feng, M. Edén, A. Brinkmann, H. Luthman, L. Eriksson, A. Gräslund, O. N. Antzutkin, and M. H. Levitt, Direct determination of a peptide torsional angle ψ by double-quantum solid state NMR, *J. Am. Chem. Soc.* **119,** 12006–12007 (1997).
15. X. Feng, P. J. E. Verdegem, Y. K. Lee, D. Sandström, M. Edén, P. Bovee-Geurts, W. J. de Grip, J. Lugtenburg, H. J. M. de Groot, and M. H. Levitt, Direct determination of a molecular torsional angle in the membrane protein rhodopsin by solid-state NMR, *J. Am. Chem. Soc.* **119,** 6853–6857 (1997).
16. P. R. Costa, J. D. Gross, M. Hong, and R. G. Griffin, Solid-state NMR measurement of Ψ in peptides: A NCCN 2Q-heteronuclear local field experiment, *Chem. Phys. Lett.* **280,** 95–103 (1997).
17. M. Hong, J. D. Gross, and R. G. Griffin, Site-resolved determination of peptide torsion angle angle ϕ from the relative orientations of backbone N–H and C–H bonds by solid state NMR, *J. Chem. Phys. B* **101,** 5869–5874 (1997).
18. S. Ravindranathan, X. Feng, T. Karlsson, G. Widmalm, and M. H. Levitt, Investigation of carbohydrate conformation in solution and in powders by double-quantum NMR, *J. Am. Chem. Soc.* **122,** 1102–1115 (2000).
19. T. Karlsson, M. Edén, H. Luthman, and M. H. Levitt, Efficient double-quantum excitation in rotational resonance NMR, *J. Magn. Reson.* **145,** 95–107 (2000).
20. E. R. Andrew, A. Bradbury, R. G. Eades, and V. T. Wynn, Nuclear cross-relaxation induced by specimen rotation, *Phys. Lett.* **4,** 99–100 (1963).
21. M. G. Colombo, B. H. Meier, and R. R. Ernst, Rotor-driven spin diffusion in natural abundance ^{13}C spin systems, *Chem. Phys. Lett.* **146,** 189–196 (1988).
22. D. P. Raleigh, M. H. Levitt, and R. G. Griffin, Rotational resonance in solid state NMR, *Chem. Phys. Lett.* **146,** 71–76 (1988).
23. M. H. Levitt, D. P. Raleigh, F. Creuzet, and R. G. Griffin, Theory and simulations of homonuclear spin pair systems in rotating solids, *J. Chem. Phys.* **92,** 6347–6364 (1990).
24. O. B. Peersen, S. Yoshimura, H. Hojo, S. Aimoto, and S. O. Smith, Rotational resonance NMR measurements of internuclear distances in an α-helical peptide, *J. Am. Chem. Soc.* **114,** 4332–4335 (1992).
25. A. E. McDermott, F. Creuzet, R. Gebhard, K. van der Hoef, M. H. Levitt, J. Herzfeld, J. Lugtenburg, and R. G. Griffin, Determination of internuclear distances and the orientation of functional groups by solid-state NMR: Rotational resonance study of the conformation of retinal in bacteriorhodopsin, *Biochemistry* **33,** 6129–6136 (1994).
26. P. R. Costa, B. Sun, and R. G. Griffin, Rotational resonance tickling: Accurate internuclear distance measurements in solids, *J. Am. Chem. Soc.* **119,** 10821–10830 (1997).
27. M. Helmle, Y. K. Lee, P. J. E. Verdegem, X. Feng, T. Karlsson, J. Lugtenburg, H. J. M. de Groot, and M. H. Levitt, Anomalous rotational resonance spectra in magic-angle spinning NMR, *J. Magn. Reson.* **140,** 379–403 (1999).
28. K. Nomura, K. Takegoshi, T. Terao, K. Uchida, and M. Kainosho, Determination of the complete structure of a uniformly labeled molecule by rotational resonance solid-state NMR in the tilted rotating frame, *J. Am. Chem. Soc.* **121,** 4064–4065 (1999).
29. S. Dusold and A. Sebald, Double-quantum filtration under rotational-resonance conditions: Numerical simulations and experimental results, *J. Magn. Reson.* **145,** 340–356 (2000).
30. T. Karlsson, M. Helmle, N. D. Kurur, and M. H. Levitt, Rotational resonance echoes in the nuclear magnetic resonance of spinning solids, *Chem. Phys. Lett.* **247,** 534 (1995).
31. T. Karlsson and M. H. Levitt, Longitudinal rotational resonance echoes in solid state nuclear magnetic resonance: Investigation of zero quantum spin dynamics, *J. Chem. Phys.* **109,** 5493–5507 (1998).
32. M. H. Levitt, The signs of frequencies and phases in NMR, *J. Magn. Reson.* **126,** 164–182 (1997).
33. M. H. Levitt and O. G. Johannessen, The signs of frequencies and phases in NMR: The role of radiofrequency mixing, *J. Magn. Reson.* **142,** 190–194 (2000).

34. G. Metz, X. Wu, and S. O. Smith, Ramped-amplitude cross polarization in magic-angle-spinning NMR, *J. Magn. Reson. A* **110,** 219–227 (1994).

35. H. Geen, M. H. Levitt, and G. Bodenhausen, Preparing initial conditions for rotational resonance in solid-state NMR spectroscopy, *Chem. Phys. Lett.* **200,** 350–356 (1992).

36. O. N. Antzutkin, Sideband manipulation in magic-angle-spinning nuclear magnetic resonance, *Prog. NMR Spectrosc.* **35,** 203–266 (1999).

37. U. Haeberlen and J. S. Waugh, Coherent averaging effects in magnetic resonance, *Phys. Rev.* **175,** 453 (1968).

38. J. Hong and G. S. Harbison, Magic-angle spinning sideband elimination by temporary interruption of the chemical shift, *J. Magn. Reson. A* **105,** 128 (1993).

39. A. E. Bennett, C. M. Rienstra, M. Auger, K. V. Lakshmi, and R. G. Griffin, Heteronuclear decoupling in rotating solids, *J. Chem. Phys.* **103,** 6951–6958 (1995).

40. R. R. Ernst, G. Bodenhausen, and A. Wokaun, "Principles of Nuclear Magnetic Resonance in One and Two Dimensions," Clarendon Press, Oxford, 1987.

41. S. Vega, Fictitious spin-1/2 operator formalism for multiple quantum NMR, *J. Chem. Phys.* **68,** 5518–5527 (1978).

42. D. K. Sodickson, M. H. Levitt, S. Vega, and R. G. Griffin, Broad band dipolar recoupling in the nuclear magnetic resonance of rotating solids, *J. Chem. Phys.* **98,** 6742–6748 (1993).

43. A. E. Bennett, J. H. Ok, R. G. Griffin, and S. Vega, Chemical shift correlation spectroscopy in rotating solids: Radio frequency-driven dipolar recoupling and longitudinal exchange, *J. Chem. Phys.* **96,** 8624–8627 (1992).

44. M. Bak, J. T. Rasmussen, and N. C. Nielsen, SIMPSON: A general simulation program for solid-state NMR spectroscopy, *J. Magn. Reson.* **147,** 296–330 (2000).

45. R. A. Haberkorn, R. E. Stark, H. van Willigen, and R. G. Griffin, Determination of bond distances and bond angles by solid-state nuclear magnetic resonance. ^{13}C and ^{14}N NMR study of glycine, *J. Am. Chem. Soc.* **103,** 2534–2539 (1981).

46. R. G. S. Spencer, K. W. Fishbein, M. H. Levitt, and R. G. Griffin, Rotational resonance with multiple-pulse scaling in solid-state nuclear magnetic resonance, *J. Chem. Phys.* **100,** 5533–5545 (1994).

47. C. E. Hughes, P. Ramasubrahmanyan, T. Karlsson, H. Luthman, and M. H. Levitt, NCCN torsional angle measurement spectroscopy using nitrogen 14, Experimental NMR Conference, Asilomar, CA, April 2000.